ARTICLE OPEN

Check for updates

Influence of Cr(III) on the formation and transformation of corrosion products of steel in marine environments

M. Serjaouan[1], C. Rémazeilles[1] and Ph. Refait[1]✉

A fundamental approach is used to better understand the influence of Cr on the resistance of low alloy steel to marine corrosion. It focuses on the formation and transformation of corrosion products of steel in seawater-like electrolytes. $Fe(OH)_2$ precipitates are then prepared by mixing a solution of NaCl, $Na_2SO_4{\cdot}10H_2O$, $FeCl_2{\cdot}4H_2O$ or $FeCl_2{\cdot}4H_2O + CrCl_3{\cdot}6H_2O$ (so that Cr = 8% and Fe = 92%), with a solution of NaOH. The initial concentration ratio of reactants, $Q = \frac{2[Fe^{2+}]+3[Cr^{3+}]}{[OH^-]}$, is set at $Q = 0.88$, 1, and 1.136. In a first approach, the obtained aqueous suspension is stirred, at a controlled temperature of 25 ± 0.5 °C, to be oxidized by air. The resulting oxidation product is characterized by XRD and Raman spectroscopy. In a second approach, the $Fe(OH)_2$ precipitates are aged one week in suspension in anoxic conditions, filtered, mixed as a wet paste with glycerol and set as a thin compact layer on the sample holder of a X-ray diffraction system. The oxidation process of $Fe(OH)_2$ is then monitored in situ during the acquisition of the X-ray diffractogram. The obtained results demonstrate that Cr(III) hinders the formation of green rust compounds, hence hindering the formation of γ-FeOOH, i.e., the main oxidation product of green rust compounds. The other oxidation pathways of $Fe(OH)_2$, which lead to Fe_3O_4 or α-FeOOH, are thus favored. Nevertheless, Cr(III) favors mainly the solid state transformation pathway of $Fe(OH)_2$, thus promoting α-FeOOH via the formation of poorly ordered Fe(III) oxyhydroxides, namely feroxyhyte and ferrihydrite.

npj Materials Degradation (2024)8:4 ; https://doi.org/10.1038/s41529-023-00424-8

INTRODUCTION

Carbon and low alloy steels are widely used for marine structures and infrastructures including sheet piles, ship hulls, off-shore platforms, and marine renewable energy devices. Steel surfaces are thus exposed worldwide to very diverse marine environments, in various exposure conditions, including the so-called atmospheric zone, splash zone, tidal zone, immersion zone, and sediment zone. The marine corrosion mechanisms are then complex, a situation aggravated by the biological activity in natural seawater that generates microbiologically influenced corrosion (MIC) processes. Even though considerable efforts were made to reach a better scientific understanding of these mechanisms, some questions remain and reference to literature data sometimes reveals apparent inconsistencies. A typical example is the influence of small compositional changes on the resistance to corrosion of low alloy steels[1].

Using the phenomenological model developed for marine corrosion of carbon and low alloy steel in the immersion zone[2–4], R. Melchers clarified some points, in particular about the role of Cr in low alloy steels[1]. In this model, two phases are distinguished, the aerobic phase, corresponding to the first years of immersion, when the corrosion rate is controlled by the diffusion of O_2, and the anaerobic phase when the corrosion process is mainly MIC, i.e., controlled by bacterial activity[4]. For low Cr contents (typically <3 wt%), the addition of Cr has a beneficial effect on resistance to corrosion during the aerobic phase, in particular if associated with Mo or Al[1]. In contrast, it has a detrimental effect during the anaerobic phase, i.e., at long term[1].

In a similar way, a recent study based on big data technology addressed the influence of Cr on atmospheric corrosion of weathering steels[5]. For low Cr contents (up to 2.56 wt%), the influence of Cr is both beneficial and detrimental. It is beneficial with respect to Cr-free steel as it increases the resistance to uniform corrosion[5]. It is detrimental because the increase in Cr content promotes pitting corrosion[5].

Numerous studies were actually devoted to the influence of Cr on the corrosion resistance of low alloy steels. In most cases, the beneficial effect, when observed, was linked to modifications of the corrosion product layer composition and morphology[6–22]. A previous study dealing with the corrosion behavior of low alloy steel in seawater confirmed that the addition of Cr (1 wt%) and Al (0.5 wt%) increased significantly the corrosion resistance of the metal in both artificial and natural seawater, at least during the aerobic phase (immersion ≤6 months)[6]. The corrosion product layer covering the steel surface at the end of the experiments was composed of two strata that could be distinguished visually, i.e., a black inner layer in contact with the steel surface, and an orange outer layer, in contact with seawater. Raman spectroscopy analysis revealed the presence, in the black inner layer, of a corrosion product characterized by a spectral signature intermediate between that of Fe_3O_4 (magnetite) and Cr_2O_3. This compound could then be a Cr-rich (Fe^{II-III},Cr^{III})-oxide. Present in the inner part of the corrosion product layer, close to the steel surface, it may play a role in the improved corrosion resistance, increasing the adhesion between the outer layer, mainly made of Fe(III)-oxyhydroxides, and the inner layer mainly composed of magnetite, green rust compounds, and Cr-containing oxide[6].

Such Fe-Cr oxides were repeatedly identified in the inner part of the corrosion product layers of Cr-containing low alloy steels immersed in saline solutions[7–10]. Other Cr-containing corrosion products were also reported, always in the inner part of the corrosion product layer, in agreement with the generally observed Cr-enrichment of the steel/corrosion product layer interface[7,11–16]. In the particular case of atmospheric corrosion, Cr-containing goethite α-$Fe_{1-x}Cr_xOOH$ was often reported[12,17–19,22]. The beneficial effect of Cr on the resistance to atmospheric corrosion was

[1]Laboratoire des Sciences de l'Ingénieur pour l'Environnement (LaSIE), UMR 7356 CNRS - La Rochelle Université, La Rochelle, France. ✉email: prefait@univ-lr.fr

often linked to the decrease in crystallinity and particle size of the FeOOH phase, which would lead to a denser and more compact, hence more protective, corrosion product layer[11,12,19–22]. The decrease in crystallinity was attributed to the substitution of Fe(III) by Cr(III) in the crystal structure of α-FeOOH[20–23]. Cr also favors the formation of goethite at the detriment of lepidocrocite[18,21], thus increasing the so-called α/γ ratio, i.e., the ratio between inactive, hence protective, phases and active, hence detrimental, phases. This effect was also reported for Cr-containing weathering steels but not necessarily associated with the presence of Cr[24]. Lepidocrocite γ-FeOOH is the typical active phase, which can be reduced to Fe(II)-bearing phases and thus participates as an oxidant to the atmospheric corrosion process, while goethite α-FeOOH is the typical inactive phase, more stable and less prone to reduction[11,25,26]. Finally, $Cr(OH)_3$ is the other Cr-containing corrosion product reported to have a beneficial effect on the resistance to corrosion of Cr-containing low alloy steels[8,16,18,20,21]. It was assumed to be the core of the nucleation of FeOOH phases and thus assumed to have a role on the decrease in FeOOH particles size[20].

However, even if the effects of Cr on composition and morphology of low alloy steel corrosion product layers were demonstrated, the fundamental mechanisms of the influence of Cr on the formation and transformation of the Fe oxides and (oxy) hydroxides were more rarely addressed[19,23,27,28]. To obtain such fundamental information, the Fe-compounds of interest are prepared in aqueous suspension and the influence of Cr on their formation and possible transformation over time is studied by replacing partially Fe by Cr. The effects of Cr on the crystallinity and local structure of α-FeOOH, or more precisely α-$Fe_{1-x}Cr_xOOH$, could be elucidated using this approach[19,23]. The influence of Cr(III) on the oxidation of the Fe(II-III) hydroxysulfate, i.e., the sulfate green rust GR_{SO4}, was assessed in a similar way[27,28]. It was observed first that Cr(III) favored the oxidation of GR_{SO4} to α-FeOOH and hindered the formation of magnetite Fe_3O_4[27]. Because GR_{SO4} is one of the main corrosion products of carbon and low alloy steels in seawater[29–32], mainly present at the steel/corrosion product layer interface, the influence of Cr(III) on both precipitation and transformation of $GR(SO_4^{2-})$ was studied[28]. The reported enrichment in Cr at this interface[7,11–16] should indeed influence the formation of the corrosion products formed directly from the Fe^{2+} ions produced by the corrosion reaction, i.e., the Fe(II)-bearing phases. It was observed that Cr(III) species decreased the crystallinity of the obtained GR_{SO4}, favored its transformation to magnetite during ageing in anoxic conditions but had no effect on its oxidation in aerated conditions[28]. This last result shows that adding Cr(III) before[28] or after[27] the formation of GR_{SO4} modifies the way Cr(III) species influence the oxidation process of the green rust.

To investigate further the modifications Cr(III) species could induce to the corrosion product layers of low alloy steel in seawater, a fundamental approach based on the study of the oxidation processes of $Fe(OH)_2$ precipitates was considered. Aqueous suspensions of $Fe(OH)_2$ were prepared, without (100 at.% Fe) or with Cr(III) (98 at.% Fe and 2 at.% Cr or 92 at.% Fe and 8 at.% Cr). With the lower Cr content, i.e., 2 at.% as in many low alloy steels, the results showed some interesting trends that were, however, not significant, difficult to interpret, and the Cr content was then increased up to 8 at.%. Therefore, the article focuses on the results obtained with 8 at.% Cr. This preliminary finding is in agreement with most previous studies showing that the influence of Cr was associated with an enrichment in Cr at the steel/corrosion product layer interface and in the inner part of this layer[7,11–16].

Two methodologic approaches were considered. First, the oxidation of the precipitate in aqueous suspension was monitored over time. The chloride and sulfate concentrations were adjusted, by adding NaCl and $Na_2SO_4 \cdot 10H_2O$, to those corresponding to seawater. The final products of the oxidation process were then characterized by X-ray diffraction (XRD) and μ-Raman spectroscopy (μ-RS). The initial precipitates were characterized by attenuated total reflection (ATR) Fourier Transform Infrared spectroscopy (FT-IR) in nitrogen atmosphere to prevent their oxidation in air. This first approach, focused on the oxidation process of aqueous suspensions of $Fe(OH)_2$, was already used previously, in particular to study the influence of chloride species[33,34], sulfate species[35,36], or both chloride and sulfate species[37] on the process. The actual corrosion processes, which take place in a thin compact layer that covers the steel surface, may, however, differ from those taking place in a stirred aerated aqueous suspension where the particles of Fe-compounds are homogeneously distributed in a large volume of liquid (200 mL in the present study).

A second approach was then considered. The initial $Fe(OH)_2$ precipitate, obtained with or without Cr(III), was filtered, and the obtained wet paste was mixed with glycerol so as to slow down, but not prevent completely, the oxidation of the $Fe(OH)_2$ particles. The resulting mixture was set in the sample holder of the XRD system, pressed to form a compact thin (~280 μm thick) layer. The evolution of the XRD pattern was monitored over time, which revealed the oxidation processes taking place inside the thin layer of $Fe(OH)_2$ particles, and the influence of Cr(III) species on these processes could be determined.

RESULTS

Oxidation in air of aqueous suspensions of $Fe(OH)_2$

The redox potential E vs time curves recorded during the oxidation of the aqueous suspensions of $Fe(OH)_2$ are displayed in Fig. 1. In any case, E initially decreases rapidly as the two solutions are mixed and $Fe(OH)_2$ precipitates. It reaches a minimal value that depends on both Q ratio and Cr proportion, but is always found approximately between −0.7 and −0.8 V vs Ag-AgCl-3M. In the absence of Cr (Fig. 1a), for $Q = 0.88$ and $Q = 1$, the potential remains in this range for about 1.1–1.2 h and increases rapidly, indicating that $Fe(OH)_2$ has been entirely oxidized to Fe(III)-based compounds, i.e., Fe_3O_4 or FeOOH compounds[33–37]. The potential then remains stable at a final value that depends on the Q ratio. The E vs time curve obtained for $Q = 1.136$ has a different shape. At the beginning, the potential stabilizes at a higher value, around −0.6 V vs Ag-AgCl-3M, and decreases after 1.3 h to reach its minimum (−0.7 V vs Ag-AgCl-3M) at time t_1. It increases slowly afterward, reaching −0.35 V vs Ag-AgCl-3M after 2.5 h, and finally increases sharply around time t_2. This shows that the oxidation process involves at least two steps, the first one corresponding to the oxidation of $Fe(OH)_2$ to a green rust (GR) compound and the second one to the oxidation of the GR compound to Fe(III)-based compounds. Actually, the formation of GR does require a Q ratio higher than 1[33–37], which explains the specific shape of the E vs time curve obtained here for $Q = 1.136$.

In a solution containing Cl^- and SO_4^{2-} ions, both chloride-GR (GR_{Cl}, i.e., $Fe^{II}_3Fe^{III}(OH)_8Cl \cdot 2H_2O$[33,34]) and sulfate-GR (GR_{SO4}, i.e., $Fe^{II}_4Fe^{III}_2(OH)_{12}SO_4 \cdot 8H_2O$[36,38]) are, however, likely to form. According to previous work[37], GR_{Cl} would form first, as it has the smallest average oxidation number for Fe of +2.25, and would be subsequently oxidized to GR_{SO4} that has a higher average oxidation number of Fe, i.e., +2.33. This was checked with a XRD analysis of the precipitate 15 min before and 15 min after t_1 (Supplementary Fig. 1), which demonstrated that GR_{Cl} was predominant before t_1 and GR_{SO4} predominant after t_1. For $Q = 1.136$, in the absence of Cr, the oxidation of $Fe(OH)_2$ is then

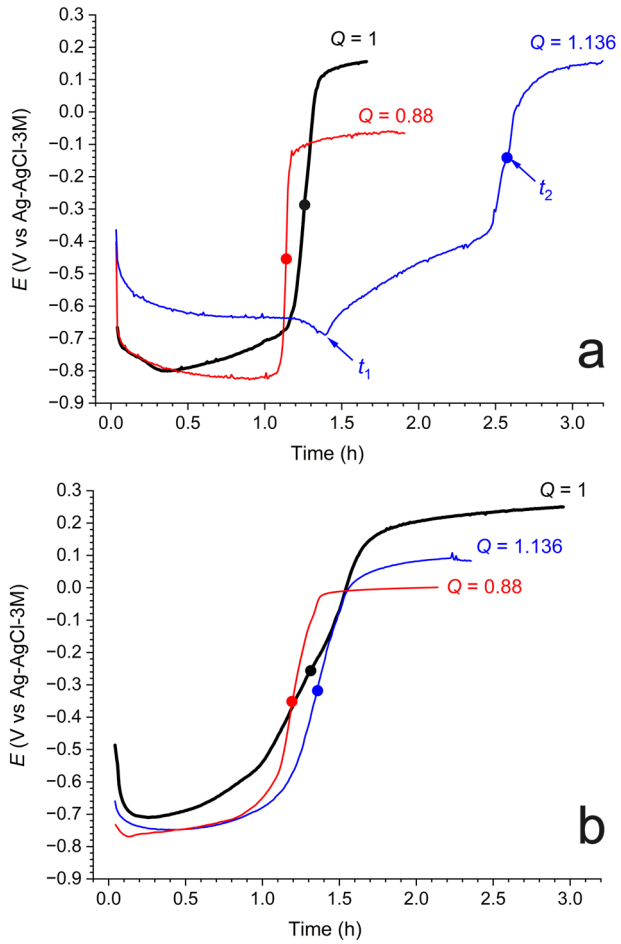

Fig. 1 Typical *E* vs. time curves obtained during the oxidation by air of $Fe(OH)_2$ aqueous suspensions, for *Q* ratios equal to 1, 1.136, 0.88. a Curves obtained in the absence of Cr(III) species. **b** Curves obtained with Cr(III) = 8 at.%. The circles point out in each curve the time t_f corresponding to the end of the oxidation reaction.

more precisely a three-step process:

$$Fe(OH)_2 \rightarrow GR_{Cl} \rightarrow GR_{SO4} \rightarrow Fe(III)-\text{based compounds}\,(Fe_3O_4 \text{ or FeOOH})$$

With 8% Cr (Fig. 1b), the three *E* vs time curves have similar shape and are rather characteristic of a one-step oxidation process. The final increase of the potential for $Q = 1$, however, involves three different slopes, as *E* increases slowly from 0.7 to 1.0 h, more rapidly between 1.0 h and 1.4 h, and abruptly between 1.4 and 1.6 h. Various oxidation processes may then take place simultaneously and end at different times. Anyway, the main change induced by Cr is observed for $Q = 1.136$ and relates to the formation of the GR compounds that Cr seems to hinder.

The overall oxidation time, t_f, was measured at the inflection point of the final sharp potential increase, as displayed in Fig. 1. For 0% Cr and $Q = 1.136$, t_f corresponds to t_2, end of the second reaction stage. For $Q = 0.88$ and $Q = 1$, t_f is only slightly increased in the presence of Cr, from 1.14 h to 1.19 h for $Q = 0.88$ and from 1.26 h to 1.28 h for $Q = 1$. Actually, the accuracy of the measured t_f values is about 10%, as determined from the scattering of values observed between 3 experiments performed in each condition. Thus, the slight variations of t_f with Cr content may not be significant. In contrast, t_f decreases from 2.58 h for 0% Cr to 1.35 h for 8% Cr, which in this case is indeed significant and clearly demonstrates that the mechanisms of oxidation and transformation of $Fe(OH)_2$ is clearly different with 8% Cr.

The final products of the oxidation process were analyzed by XRD (Figs. 2 and 3) and μRS (Fig. 4). The XRD patterns of Fig. 2 relate to the oxidation without Cr. For each *Q* value, only one phase is observed, and the nature of this phase depends on *Q*. These final oxidation products are magnetite Fe_3O_4 for $Q = 1$, goethite α-FeOOH for $Q = 0.88$, and lepidocrocite γ-FeOOH for $Q = 1.136$. This result is consistent with previous works[33,35] and illustrates the importance of the *Q* ratio, which was interpreted as follows: Goethite is favored for $Q < 1$, i.e., when an excess of OH^- ions remains in solution after the precipitation of $Fe(OH)_2$, because its formation is favored in alkaline conditions (pH measured at 11.5–12, once stabilized a few minutes after precipitation). Lepidocrocite is favored for $Q > 1$ because it is the phase that forms preferentially from GR compounds, and magnetite is favored when neither OH^- nor Fe^{2+} ions remain in excess after the precipitation of $Fe(OH)_2$, i.e., when $Q = 1$. Note that the pH of the suspension decreases when *Q* increases. It was measured at 9.5–10.0 for $Q = 1$ and at 7.5–8.0 for $Q = 1.136$, once stabilized after precipitation.

The XRD patterns obtained with 8% Cr are displayed in Fig. 3. Significant differences are observed with the previous patterns, which demonstrate that this Cr proportion can have an important effect on the formation of Fe-corrosion products. First, for $Q = 1$, the main oxidation product is now goethite, and magnetite is observed as a minor phase, as only its two main diffraction peaks, M311 and M440, can be seen. This result shows that Cr favors the formation of goethite, as observed previously via the characterization of the rust layer covering Cr-bearing low alloy steel after atmospheric corrosion[18]. For $Q = 1.136$, the three phases, i.e., lepidocrocite, magnetite and goethite are formed, and none of them predominates. If Cr hinders the formation of GR compounds, as suggested by the corresponding *E* vs time curve, then it subsequently hinders the formation of lepidocrocite, which is favored when GR is formed as a transient oxidation product. Consequently, the formation of other compounds, i.e., magnetite and goethite, is favored. Finally, for $Q = 0.88$, goethite is, as in the absence of Cr, the only oxidation product of $Fe(OH)_2$. Comparing closely both diffractograms, it can be seen that the diffraction lines of goethite are broader in the absence of Cr. The determination of the full width at half maximum (FWHM) of the diffraction lines by computer fitting (using Gauss functions) confirmed it. For the intense G110 peak, for instance, FWHM is 1.65° without Cr and 1.12° with 8% Cr. This indicates that, in our experimental conditions, Cr not only favor the formation of goethite with respect to magnetite and lepidocrocite, but it also favors the growth and/or increase the crystallinity of goethite particles. Various previous works dealing with atmospheric corrosion indicated that, conversely, FeOOH crystallinity and particle size were decreased for Cr-bearing low alloy steel[11,12,19–22]. However, the increase in crystallinity and/or particle size observed here for $Q = 0.88$ correspond to particular pH conditions, i.e., alkaline conditions (pH about 11.5–12), which do not correspond to pH conditions typical of atmospheric corrosion.

μ-RS analysis confirmed the results given by XRD. As an example, a selection of the Raman spectra obtained with Cr = 8% at $Q = 1$ and $Q = 1.136$ is displayed in Fig. 4. All the spectra obtained for $Q = 1$ mainly show the Raman bands of goethite[39,40], at (with decreasing intensity) 390, 300, 480, 555, and 249 cm^{-1}, and the main Raman peak of magnetite at 670 cm^{-1} [39,40]. The peak at 700–705 cm^{-1} may be attributed to ferrihydrite[41], a poorly ordered and poorly crystallized Fe(III)-oxyhydroxide phase difficult to detected by XRD. For $Q = 1.136$, the main peaks of goethite and magnetite are seen again, now with those of lepidocrocite, at 252, 380, and 528 cm^{-1} [39,40].

To illustrate the results obtained with 2% Cr, the XRD pattern and three typical Raman spectra of the end products of the oxidation for $Q = 1$ are displayed in Fig. 5. The XRD pattern reveals, as for 8% Cr, that both magnetite and goethite were

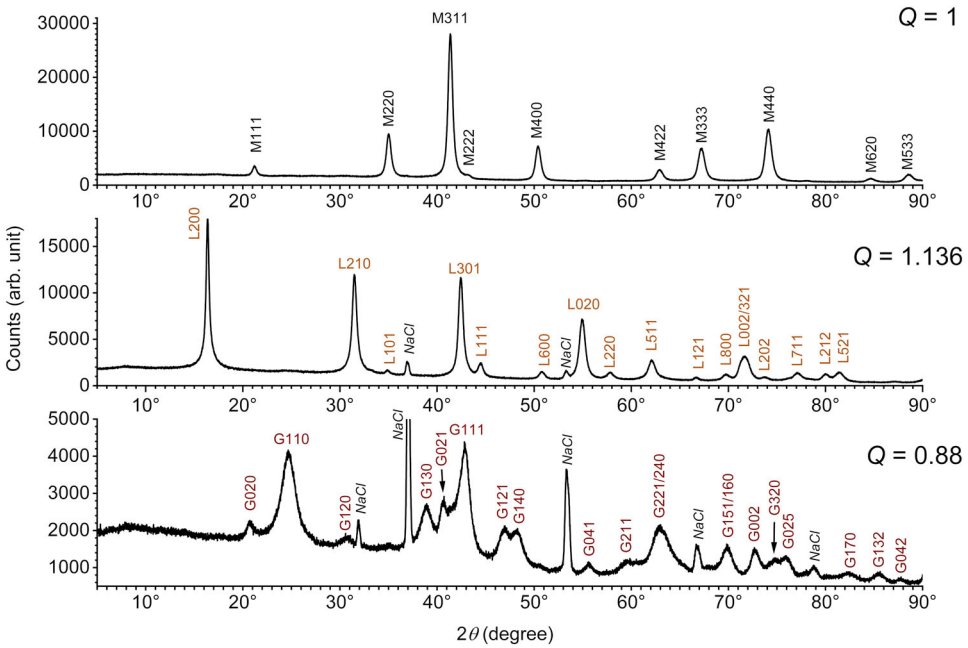

Fig. 2 XRD patterns (Co-Kα wavelength) of the final products of the oxidation by air of $Fe(OH)_2$ aqueous suspensions obtained in the absence of Cr(III) species for *Q* ratios equal to 1, 1.136, and 0.88. G are the diffraction peaks of goethite, L those of lepidocrocite and M those of magnetite, denoted with the corresponding Miller index.

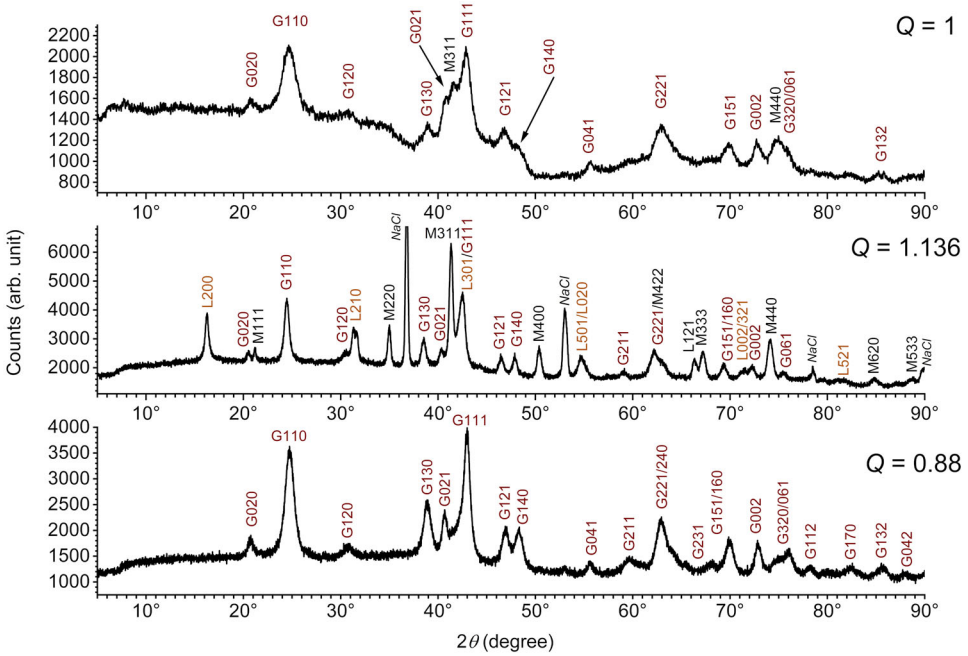

Fig. 3 XRD patterns (Co-Kα wavelength) of the final products of the oxidation by air of $Fe(OH)_2$ aqueous suspensions obtained with Cr(III) = 8 at.% for *Q* ratios equal to 1, 1.136, and 0.88. G are the diffraction peaks of goethite, L those of lepidocrocite and M those of magnetite, denoted with the corresponding Miller index.

formed, but goethite as a minor component in this case. This is confirmed by Raman analysis. The three displayed spectra, obtained with different zones of the sample, are similar. The main Raman peak of magnetite at 670 cm^{-1} is clearly predominant while the two other minor peaks, at 300 and 550 cm^{-1}, are also visible[39,40]. Only the main Raman peak of goethite is visible, at 390 cm^{-1} [39,40] and its intensity is similar to that of the smallest peaks of magnetite. In conclusion, the influence of 2% Cr remains the same as that observed with 8 at.% Cr, but the effects are much smaller.

FT-IR spectroscopy of 1-week aged $Fe(OH)_2$ precipitates

The FT-IR spectra of the 6 considered aqueous suspensions are gathered in Fig. 6. First, it can be noted that even if the procedure involves a drying of the samples in a N_2 flow, water molecules cannot be entirely removed, as some molecules are bound to the solid particles surfaces. For the samples prepared without Cr, the persistence of a small amount of water molecules is revealed by a flat broad band around 3400 cm^{-1}, corresponding to the O-H stretching mode, and a very small peak at 1630 cm^{-1} (O-H

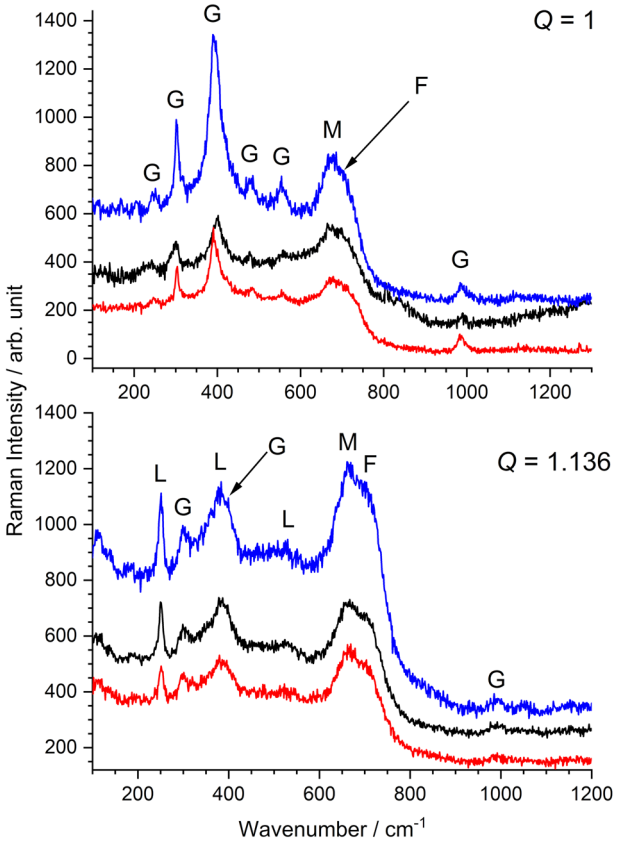

Fig. 4 Typical Raman spectra of the final products of the oxidation by air of $Fe(OH)_2$ aqueous suspensions obtained with Cr(III) = 8 at.% for *Q* ratios equal to 1 and 1.136. G are the Raman peaks of goethite, L those of lepidocrocite and M those of magnetite.

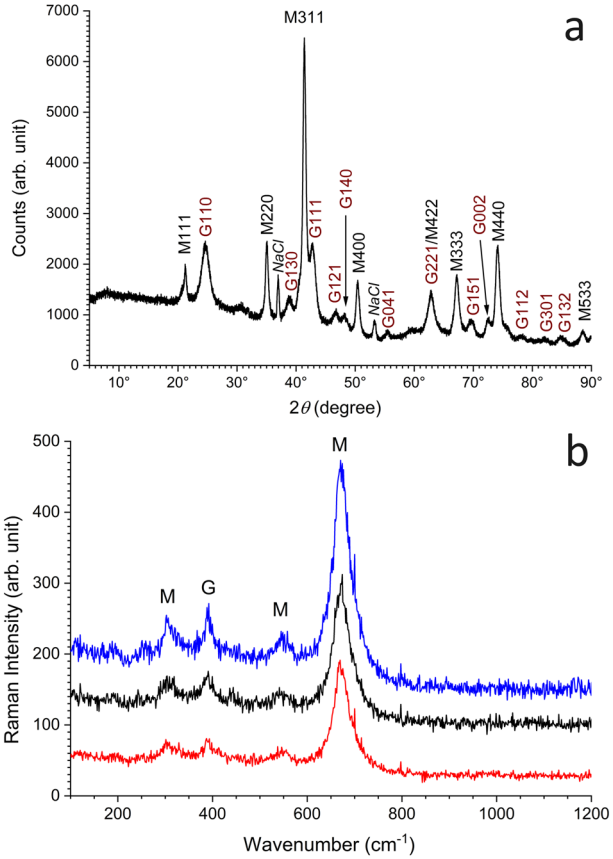

Fig. 5 Characterization of the final products of the oxidation by air of $Fe(OH)_2$ aqueous suspensions obtained with Cr(III) = 2 at.% for *Q* equal to 1. a XRD pattern. **b** Typical Raman spectra. G are the peaks of goethite and M those of magnetite, denoted with the corresponding Miller index in the XRD pattern.

deformation mode)[42]. The spectral signature of H_2O molecules is accompanied by that of sulfate species, that corresponds to a doublet of peaks at 1120 cm^{-1} and 1150 cm^{-1} [43]. However, for the samples prepared with 8% Cr, the vibration bands of H_2O are much more intense, indicating that the precipitate remained largely hydrated, i.e., that particles of the solid phases formed a gel-like matrix, retaining part of the electrolyte, as revealed by the concomitant increase of the signal of both water molecules and sulfate species. The solid phase precipitating in the absence of Fe, i.e., for 100% Cr and $Q = 1$, was prepared in the same conditions and analyzed by XRD (Supplementary Fig. 2). It revealed mostly amorphous and/or nanocrystalline matter, but some diffraction peaks were, however, clearly seen. They corresponded to $Cr(OH)_3 \cdot 6H_2O$, i.e., a hydrated Cr(III) hydroxide. The OH^- ions associated with $Cr(OH)_3$ should give rise to an additional O-H stretching signal, and, looking closely to the corresponding FT-IR spectra, a shoulder is visible around 3000 cm^{-1}, on the low wavenumber side of the broad band mainly due to H_2O molecules. This shoulder is more pronounced for $Q = 0.88$. The hydrogen bond between H atoms of hydroxide ions of both $Fe(OH)_2$ and $Cr(OH)_3$ and O atoms of water molecules should also give a signal in this spectral region.

The other detected peaks, at 3627 and 487 cm^{-1}, are those typical of the Fe(II) hydroxide[44]. The peak at 3627 cm^{-1} is sharp and corresponds to the O-H stretching mode while the peak at 487 cm^{-1} corresponds to a lattice (T′) mode[44]. Actually, this second peak is exactly at 487 cm^{-1} for $Fe(OH)_2$ obtained without Cr but shifted to a slightly higher wavenumber, about 502 cm^{-1}, for $Fe(OH)_2$ obtained with 8% Cr. A similar shift of this vibration band to 505–508 cm^{-1} was observed previously for partly oxidized $Fe(OH)_2$[44], i.e., it is associated with the presence of Fe(III) in the crystal lattice of $Fe(OH)_2$. In the present case, this systematic shift observed with 8% Cr can be attributed to the presence of Cr(III) ions in the lattice of $Fe(OH)_2$.

The precipitation of a hydrated Cr(III) hydroxide together with $Fe(OH)_2$ can explain partially the stronger H_2O signal of the FT-IR spectra, but not that of the sulfate ions. This very intense H_2O signal, associated with a similarly intense sulfate signal, shows that $Cr(OH)_3$ actually helped forming a gel-like structure that not only retains the water molecules bound to the $Cr(OH)_3$ matrix, but sulfate ions as well (and more likely Na^+ and Cl^- ions that cannot be evidenced with FT-IR spectroscopy).

Consequently, FT-IR analysis of the precipitates after 1 week of ageing in anoxic conditions demonstrates that the only Fe-bearing phase was $Fe(OH)_2$ whereas Cr(III) appears to be present both as a hydrated $Cr(OH)_3$ phase and as Cr^{3+} ions present in the crystal lattice of $Fe(OH)_2$. Note that $Cr(OH)_3$ is actually a phase repeatedly identified in the corrosion product layers covering Cr-containing low alloy steels[8,16,18,20,21].

XRD monitoring of compact thin layers of $Fe(OH)_2$

A schematic representation of the thin layers analyzed with this methodologic approach is displayed in Fig. 7. The precipitate, aged 1 week in anoxic conditions, was not filtered and thoroughly dried, but filtered to a wet paste and mixed as such with glycerol. The resulting oily paste was spread on the sample holder to form a dense thin (280 µm) layer. Consequently, the particles of $Fe(OH)_2$, represented here as hexagons according to the crystal structure[44], are partly surrounded by water and partly surrounded by glycerol. This procedure limited the oxidation of $Fe(OH)_2$ without

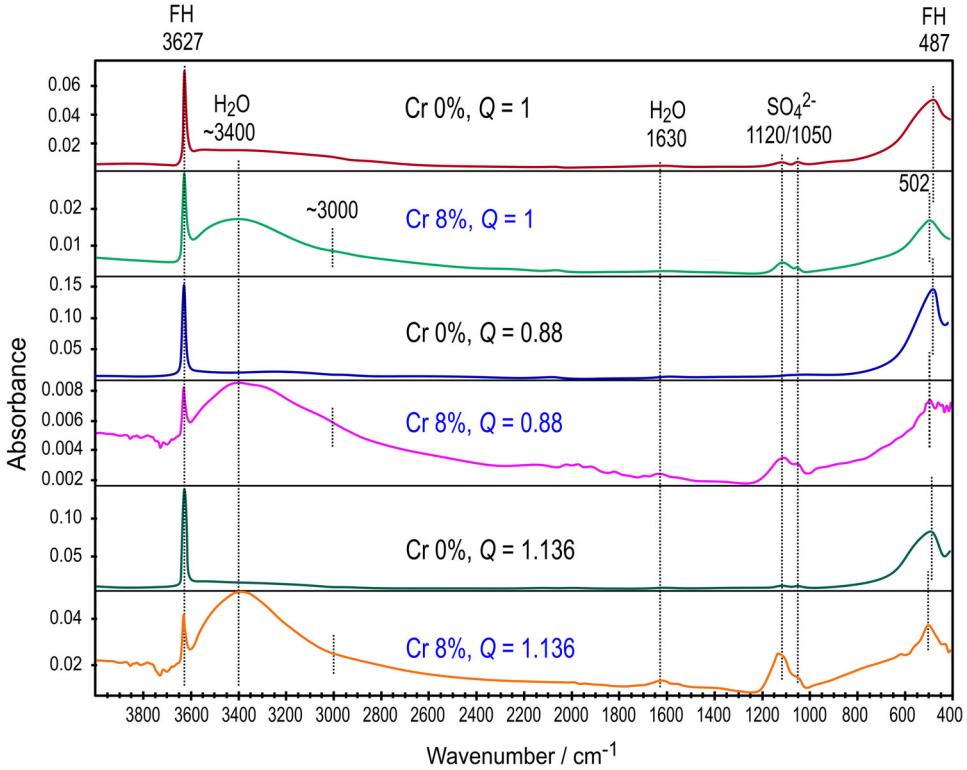

Fig. 6 FT-IR spectra of $Fe(OH)_2$ precipitates obtained without Cr(III) species or with 8 at.% Cr(III), for Q ratios equal to 1, 0.88, and 1.136, after 1 week of ageing at RT in anoxic conditions and drying under a N_2 flow.

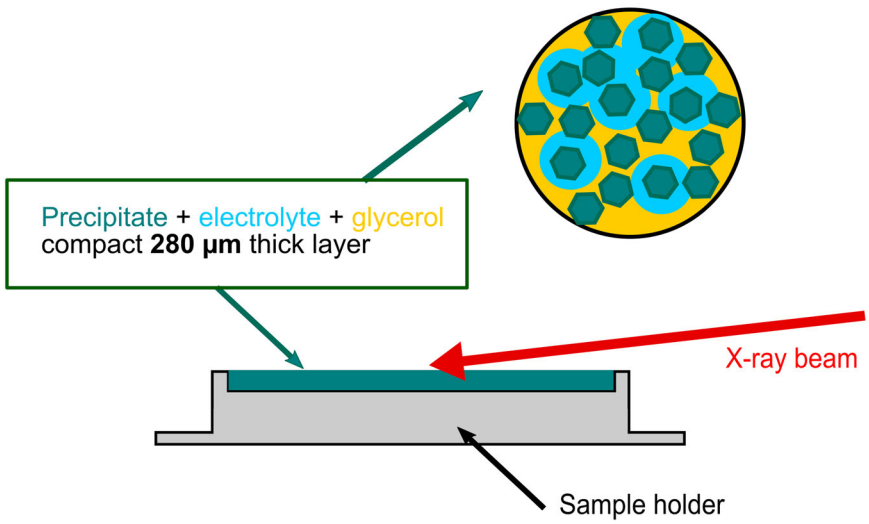

Fig. 7 Schematic representation of the thin compact layers of $Fe(OH)_2$ used for the in situ XRD monitoring of the oxidation process.

preventing it completely. Preliminary tests demonstrated that the wetter the filtered paste was before mixing with glycerol, the higher was the oxidation rate of $Fe(OH)_2$ during the acquisition of the XRD pattern. The acquisition time was restricted to 30 min as it was visually observed that the analyzed sample was almost dry, i.e., only solid phases and glycerol remained present, after such duration of exposure to the X-ray beam.

The results obtained with $Fe(OH)_2$ precipitates prepared without Cr at $Q = 1$ and $Q = 0.88$ are summarized in Fig. 8. Depending on the quality of the XRD pattern, the first pattern was recorded after 30 s ($Q = 0.88$) or 3 min ($Q = 1$). In both cases, this first pattern only revealed the presence of the characteristic diffraction peaks of $Fe(OH)_2$, in agreement with FT-IR analysis. These peaks are only accompanied by a broad band, centered on $2\theta = 26°$, which is due to glycerol[45]. This signal is clearly visible on the pattern recorded after 3 min for $Q = 1$. Then, oxidation products of $Fe(OH)_2$ were progressively revealed. For $Q = 1$, the main oxidation product proved to be the chloride green rust, GR_{Cl}, and its four main peaks could then be distinguished on the pattern recorded after 30 min. At the end of the experiment, two additional very small peaks could be seen, and are attributed to feroxyhyte, i.e., δ-FeOOH. For $Q = 0.88$, feroxyhyte was the only oxidation product to form.

Feroxyhyte forms when dissolution-reprecipitation processes cannot take place. It is commonly obtained via a violent oxidation

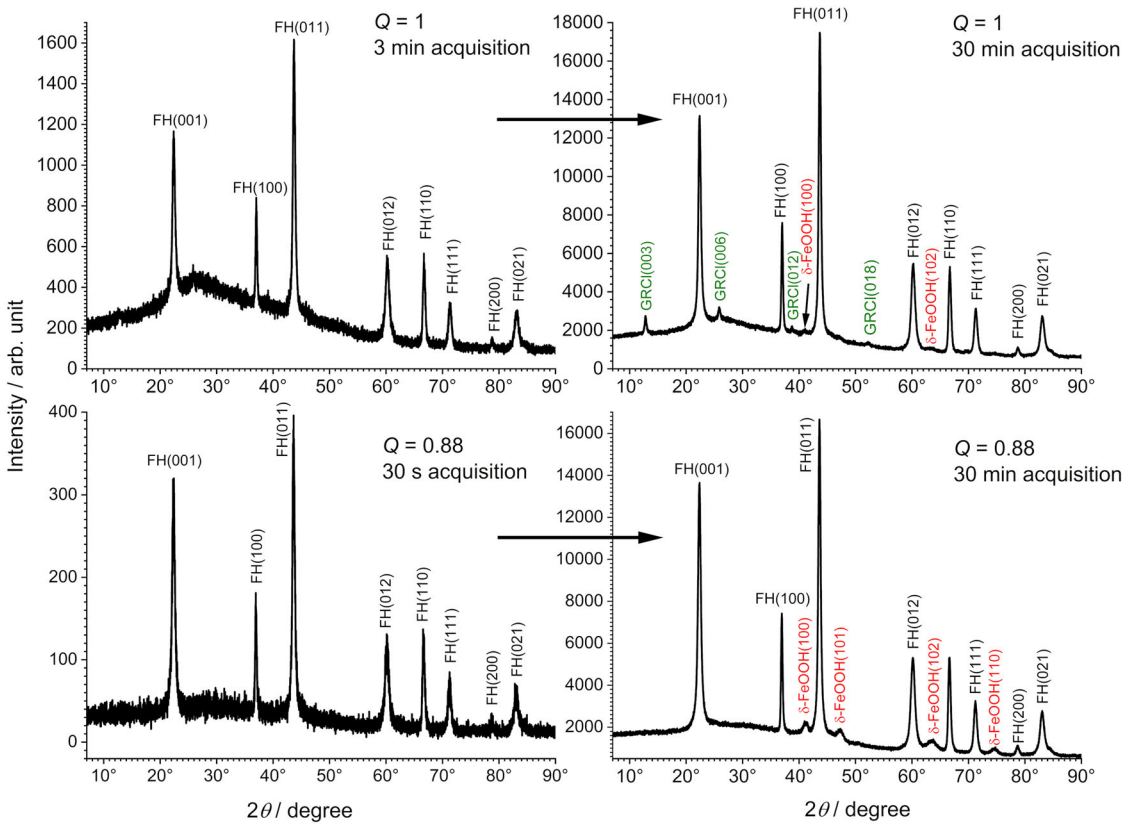

Fig. 8 XRD patterns (Co-Kα wavelength) of thin layers of $Fe(OH)_2$ obtained in the absence of Cr(III) species for Q ratios equal to 1 and 0.88, acquired after 30 s ($Q = 0.88$) or 3 min ($Q = 1$), and 30 min for both Q ratios. FH are the diffraction peaks of $Fe(OH)_2$, GRCl those of the chloride-GR, and δ-FeOOH those of feroxyhyte, denoted with the corresponding Miller index.

of $Fe(OH)_2$[46,47], e.g., using hydrogen peroxide. It is structurally similar to its precursor phase $Fe(OH)_2$ in the sense that it keeps the hexagonal close packing of anions[46–48]. It can also be obtained by other methods implying that a solid state transformation takes places, and for instance can be obtained by exposure of dried $Fe(OH)_2$ to oxygen[47]. Therefore, in our experiments, feroxyhyte could result from the oxidation of the $Fe(OH)_2$ particles remaining unoxidized after the evaporation of water. This would explain its formation at the end of the experiment for $Q = 1$. However, a phase structurally similar to δ-FeOOH, which was called α′-FeOOH, was identified as the precursor phase to goethite α-FeOOH in the oxidation process of $Fe(OH)_2$ in alkaline conditions[35,49]. Based on the characteristic XRD pattern of feroxyhyte, now commonly admitted to be composed of four diffraction peaks, i.e., (100), (101), (102), and (110) as illustrated in Fig. 8 for $Q = 0.88$, α′-FeOOH and δ-FeOOH are actually the same compound. Besides, the more recent study about the crystal structure of δ-FeOOH demonstrated that feroxyhyte shared key structural features with goethite[50]. Older works also emphasized that the transformation of δ-FeOOH to α-FeOOH only required a re-arrangement, or a re-ordering, of Fe^{3+} cations in the octahedral sites of the hexagonal close packing of O atoms[46]. Thus, feroxyhyte must be considered as a precursor of the formation of goethite, which explained why it is obtained as the only oxidation product in the early stages of the process for $Q = 0.88$, i.e., a process that led, for the corresponding aqueous suspension, to goethite (Fig. 2).

Figure 9 displays the XRD patterns obtained for a $Fe(OH)_2$ precipitate prepared without Cr at $Q = 1.136$. Three patterns are displayed. The first one, recorded after 30 s, shows that GR_{Cl} is present, as a minor phase, together with $Fe(OH)_2$. GR_{Cl} was not be detected by FT-IR spectroscopy, more likely because its signal was too weak. It is also possible that GR_{Cl} formed during the filtration procedure but it was systematically and only observed in these conditions (i.e., Cr = 0% and $Q = 1.136$). The other assumption is that the small initial amount of Fe(III), present because the solutions were not deaerated, induced the formation of GR_{Cl} during precipitation, as the formation of GR compounds is favored for $Q > 1$[33,35]. Then, after 3 min of experiment, the main peaks of the sulfate green rust GR_{SO4} were in turn clearly visible. As the oxidation process went on, the intensity of the diffraction peaks of GR_{SO4} increased, relatively to those of $Fe(OH)_2$ and GR_{Cl}. This process is similar to that observed with the aqueous suspensions, i.e., $Fe(OH)_2$ is first oxidized to GR_{Cl} which is in turn oxidized to GR_{SO4}. Finally, as for the other Q ratios, feroxyhyte was also obtained after 30 min.

The results obtained for precipitates prepared with 8% Cr are summarized in Fig. 10. Only the patterns obtained after 30 min are displayed because those recorded after 30 s or 3 min were similar, whatever the acquisition time and the Q ratio, and only showed the diffraction peaks of $Fe(OH)_2$. As revealed by the XRD patterns finally obtained, this is due to the fact that the formation of green rust compounds did not take place. Consequently, feroxyhyte was the only observed oxidation product, may be accompanied by another poorly crystallized Fe(III) compound. Two additional weak broad peaks can be seen for $Q = 1.136$, and maybe for $Q = 0.88$. These broad diffraction peaks may correspond to so-called "2-line" ferrihydrite[51], the most poorly ordered and poorly crystallized form of Fe(III)-(oxy)hydroxides. This results clearly demonstrates that Cr(III) hinders the oxidation of $Fe(OH)_2$ to green rust compounds.

The XRD data were also used to study the morphology of the $Fe(OH)_2$ particles. Using the XRD patterns obtained after 30 min of acquisition, the 6 main diffraction peaks of $Fe(OH)_2$ were computer fitted with Gauss functions to determine the angular

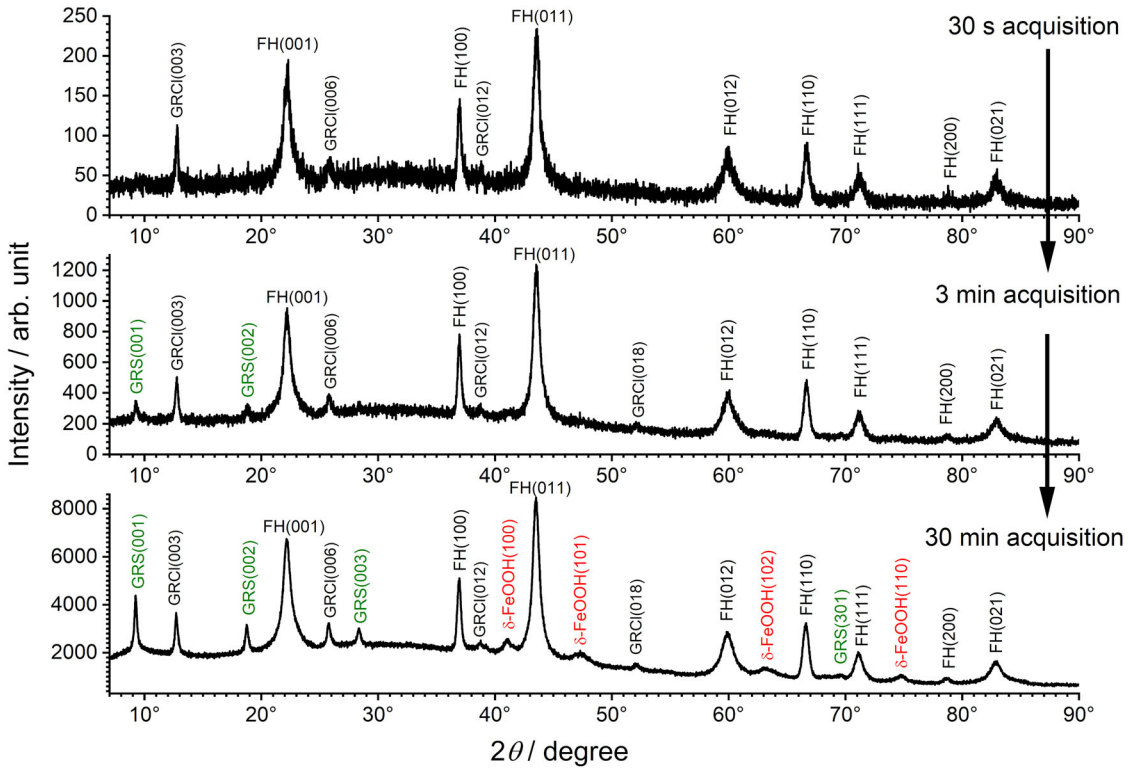

Fig. 9 XRD patterns (Co-Kα wavelength) of thin layers of $Fe(OH)_2$ obtained in the absence of Cr(III) species for $Q = 1.136$, acquired after 30 s, 3 min, and 30 min. FH are the diffraction peaks of $Fe(OH)_2$, GRCl those of the chloride-GR, GRS those of the sulfate-GR, and δ-FeOOH those of feroxyhyte, denoted with the corresponding Miller index.

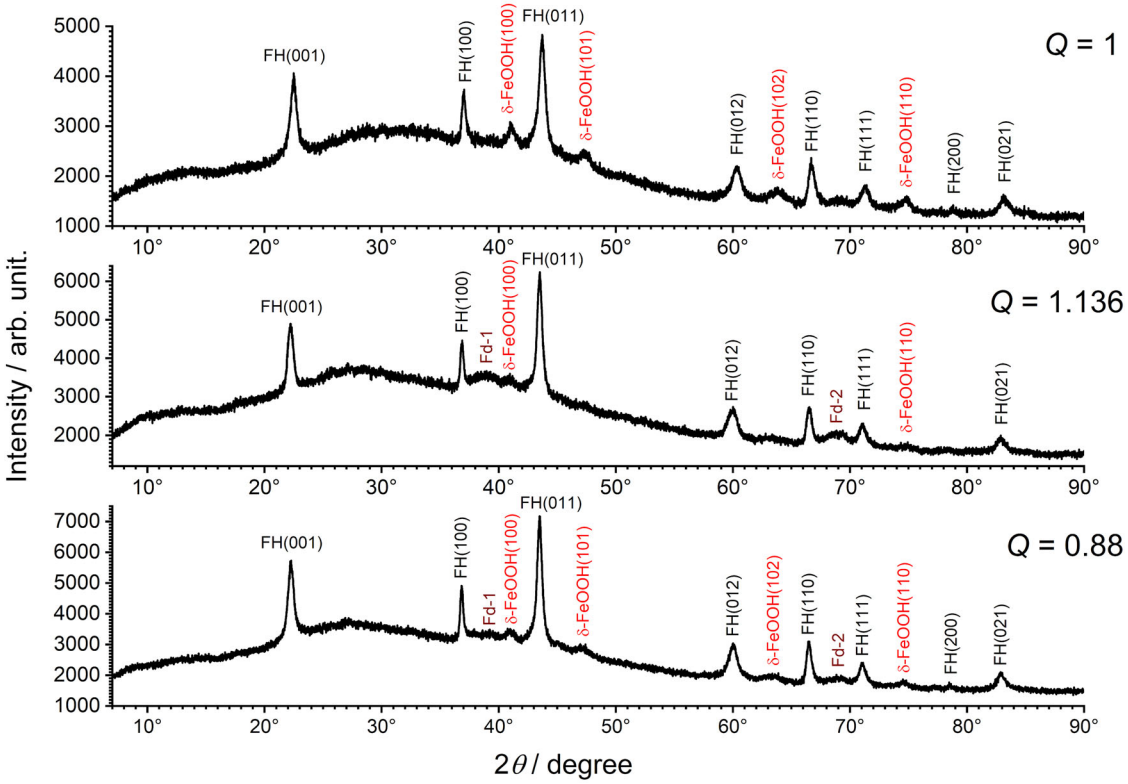

Fig. 10 XRD patterns (Co-Kα wavelength) of thin layers of $Fe(OH)_2$ obtained with 8 at.% of Cr(III) for Q ratios equal to 1, 0.88, and 1.136, for an acquisition time of 30 min. FH are the diffraction peaks of $Fe(OH)_2$ and δ-FeOOH those of feroxyhyte, denoted with the corresponding Miller index. Fd-1 and Fd-2 correspond to ferrihydrite.

Table 1. XRD data for the 6 main peaks of $Fe(OH)_2$ at $Q = 1$ (30 min. acquisition), 0% Cr and 8% Cr: d_{hkl} is the interplanar distance, I_{hkl} is the intensity of the corresponding diffraction peak (with 100 for the main one) and D_{hkl} is the particle size in the direction perpendicular to the hkl planes.

Diffraction peak	0%Cr			8%Cr			Reference I_{hkl} values[a]
	d_{hkl} (Å)	I_{hkl}	D_{hkl} (Å)	d_{hkl} (Å)	I_{hkl}	D_{hkl} (Å)	
001	4.605	77	250	4.590	67	175	66
100	2.818	24	700	2.817	24	500	32
011	2.404	100	310	2.403	100	190	100
012	1.783	46	160	1.78	36	145	38
110	1.627	29	330	1.626	33	260	20
111	1.535	19	240	1.535	17	215	12

[a]Values taken from the ICDD PDF-4 data file #01-073-6991.

position, the intensity, and the full width at half maximum of each peak. The width of the peak was used to determine the particle size using the Sherrer equation. Table 1 gives the data obtained for $Q = 1$ at both Cr contents.

The obtained relative intensities of the diffraction peaks can first be compared to those expected for randomly orientated particles (reference I_{hkl} values in Table 1). No significant differences are observed, which indicates that the $Fe(OH)_2$ particles are indeed randomly orientated inside the 280 µm thick analyzed layer. Looking at the dimension of the particles, it can first be seen that these particles are significantly smaller with 8% Cr. The interplanar distances are similar, except d_{001} that is significantly smaller with Cr. Due to the smaller size of Cr^{3+} ions with respect to Fe^{2+} ions[52], the presence of Cr^{3+} in the crystal structure of $Fe(OH)_2$ could indeed lead to the decrease in the lattice cell size. It could also explain the observed decrease in particle size. Actually, FTIR analysis already indicated that part of the Cr^{3+} ions were present inside the crystal structure of $Fe(OH)_2$.

As for the shape of the $Fe(OH)_2$ particles, it can be noted that D_{001}, i.e., the dimension along the basal plane, is much higher (approximately three times as much) than D_{100}, i.e., the dimension along the *c* axis of the hexagonal layered structure of $Fe(OH)_2$. The $Fe(OH)_2$ particles may be hexagonal platelets, as represented in Fig. 7, but they are thick ones.

DISCUSSION

If the corrosion process is uniform, both anodic and cathodic reaction rates are identical at each point of the steel surface. For a Cr-containing low alloy steel, the anodic reaction can be written, with *x* measuring the amount of Cr atoms oxidized per oxidized Fe atom, as:

$$FeCr_x \rightarrow Fe^{2+} + xCr^{3+} + (2+3x)e^- \quad (1)$$

Assuming the cathodic reaction is O_2 reduction, if the same number of electrons is involved, then the reaction is:

$$\left(\frac{1}{2}+\frac{3x}{4}\right)O_2 + \left(1+\frac{3x}{2}\right)H_2O + (2+3x)e^- \rightarrow (2+3x)OH^- \quad (2)$$

In this case, when 1 Fe^{2+} and *x* Cr^{3+} cations are produced by the anodic reaction, $(2+3x)$ OH^- ions are simultaneously produced by the cathodic reaction. Then, the ratio *Q* (see Eq. 3 in the "Methods" section) is equal to 1. Consequently, in anodic zones of the surface where Fe^{2+} and Cr^{3+} cations are in excess with respect to OH^- ions, *Q* is larger than 1, while in cathodic zones where OH^- ions are in excess, *Q* is smaller than 1. As *Q* has a strong influence on the obtained corrosion products, the composition of the corrosion product layer may differ in anodic and cathodic zones. This phenomenon was clearly observed for carbon steel immersed in seawater, and it was shown that magnetite was favored in cathodic zones while GR_{SO4} and FeOOH were favored in anodic zones[31,32]. The influence of Cr may then be different in anodic zones ($Q > 1$), cathodic zones ($Q < 1$) or if the process is uniform and does not involve persistent anodic and cathodic areas ($Q = 1$).

The combination of two methodologic approaches, one based on the oxidation of $Fe(OH)_2$ aqueous suspensions, the other based on the XRD monitoring of the oxidation of thin layers of $Fe(OH)_2$, revealed various effects of Cr(III) on the formation of Fe-corrosion products in marine environments and the associated mechanisms.

One of the effects of Cr(III) on the oxidation processes of $Fe(OH)_2$ is to hinder the formation of GR compounds. Actually, in a comparative study of marine corrosion processes of 2.2% Cr low alloy steel and mild steel, it was observed that the predominant compounds in the inner stratum of the corrosion product layers obtained after 320 days of immersion in natural seawater differed significantly[53]: For mild steel, the main components of the inner stratum were GR compounds and amorphous FeS. For 2.2% Cr low alloy steel, the main components were various iron sulfides, and green rust compounds were not identified. The authors did not comment on that particular point but their results confirm that chromium has a negative impact on GR formation.

The FT-IR analysis of the initial precipitates revealed that Cr^{3+} ions were mainly present as a hydrated $Cr(OH)_3$ compound forming a gel-like structure hence binding water molecules and ions from the solution to the solid phases. FT-IR also revealed that part of the Cr^{3+} ions were present in the crystal lattice of $Fe(OH)_2$. The in situ XRD monitoring of the oxidation of thin layers of $Fe(OH)_2$ clearly revealed that the oxidation process leading to GR compounds was inhibited by Cr(III), which led to the formation of feroxyhyte δ-FeOOH and a compound similar to ferrihydrite, both phases corresponding to poorly ordered forms of Fe(III)-(oxy) hydroxides. Feroxyhyte is the oxidation product of $Fe(OH)_2$ when dissolution-reprecipitation processes cannot occur, because δ-FeOOH is obtained from $Fe(OH)_2$ via a solid state transformation. This result shows that the formation of GR compounds is hindered by Cr(III) because dissolution-reprecipitation processes are hindered. This phenomenon may be attributed to the gel-like $Cr(OH)_3$ matrix because the water molecules it retains, which also surround the $Fe(OH)_2$ crystallites, are bound to the solid phase. The formation of $Cr(OH)_3$, commonly reported for Cr-containing low alloy steel[8,16,18,20,21], seems then to be a key point in the mechanisms involved in the beneficial effect of Cr on the resistance to corrosion of these alloys.

Both ferrihydrite and feroxyhyte are metastable Fe(III)-compounds and precursors of goethite. The inhibition of dissolution-precipitation processes due to the $Cr(OH)_3$ gel-like matrix necessarily hinders the transformation of both phases and the growth of the finally obtained goethite particles. Consequently, Cr(III) would globally favor the formation of smaller FeOOH particles, which was indeed often reported for Cr-containing low alloy steels, in particular for atmospheric corrosion[11,12,19–22]. This result was not obtained during the study of $Fe(OH)_2$ in aqueous suspension. However, the effect of the $Cr(OH)_3$ gel-like matrix may be much less important for $Fe(OH)_2$ particles scattered in a large volume of solution. Reported effects of Cr(III) such as densification of the rust layer cannot indeed be observed with the methodology based on oxidation of aqueous precipitates but may be revealed with the new approach proposed here, i.e., the in situ XRD monitoring of the oxidation of dense thin layers of $Fe(OH)_2$ precipitates.

Note also that the presence of some Cr^{3+} ions in the crystal lattice of $Fe(OH)_2$, as indicated by both FT-IR analysis and XRD analysis, implies that goethite finally obtained is Cr-substituted

goethite, considering in particular that goethite is obtained via a solid state transformation.

Finally, the last point is the formation of feroxyhyte δ-FeOOH, obtained in any case during the in situ XRD monitoring of the oxidation of thin layers of $Fe(OH)_2$. In the absence of Cr(III), feroxyhyte more likely formed after the complete evaporation of the aqueous liquid phase. During an atmospheric corrosion process, it could form similarly at the end of the drying periods, when $Fe(OH)_2$ particles, whether formed by the corrosion of steel or resulting from the reduction of FeOOH phases, are found in a dry state, no more surrounded by any electrolyte. Poorly crystallized or (sometimes called amorphous) FeOOH phases were reported as an important component of the rust layer resulting from atmospheric corrosion[22,24–26,41,54]. For Cr-containing low alloy steel, the formation of phases such as ferrihydrite and feroxyhyte, both observed during the in situ XRD monitoring of the oxidation of thin layers of $Fe(OH)_2$, should be favored even during the wet period, because of the positive effect of Cr(III) on the solid state transformation pathway. As already noted, it was repeatedly reported that the rust layers of Cr-containing low allow steels subjected to atmospheric corrosion contained a higher proportion (with respect to carbon steel) of poorly crystallized/small sized particles of FeOOH phases[11,12,19–22].

The study of the oxidation of aqueous suspensions gave fundamental information. First, the results obtained with $Fe(OH)_2$ precipitates without Cr illustrate the three main pathways for the oxidation of $Fe(OH)_2$, that led to the most common corrosion products of iron and steel, i.e., lepidocrocite, goethite, and magnetite, depending on the ratio Q. For $Q = 0.88$, i.e., in alkaline conditions, $Fe(OH)_2$ was oxidized to goethite. According to previous work[35], goethite is obtained via a precursor similar to δ-FeOOH for ratios around $Q = 0.83$. As δ-FeOOH is obtained from $Fe(OH)_2$ via a solid state transformation, this suggests that, for $Q = 0.88$, this transformation mechanism was favored due to the lower solubility of $Fe(OH)_2$ in alkaline conditions. According to thermodynamic data[55], the solubility of $Fe(OH)_2$ is the lowest around pH = 12, which corresponds to the conditions met for $Q = 0.88$. At such pH, the activity of Fe(II) dissolved species in equilibrium with the solid phase is very low, smaller than 10^{-7}.

In contrast, for $Q = 1.136$, in the presence of excess dissolved Fe(II) species, dissolution-reprecipitation processes are favored and lepidocrocite is obtained via the formation of GR compounds as intermediate transient compounds. For $Q = 1$, a specific mechanism leading to magnetite, discussed in previous studies[35], takes place.

Secondly, with 8% of Cr(III), it is observed that, for $Q = 1.136$, lepidocrocite is not the only oxidation product, as magnetite and goethite are obtained too. This shows that even in aqueous suspensions, Cr(III) partially hinders the transformation pathways involving GR compounds and then lepidocrocite. Consequently, the two other transformation pathways can take place, leading to goethite and magnetite. For $Q = 1$, magnetite is not the only oxidation product and goethite is mainly obtained. This shows that Cr(III) favors the formation of goethite, because it favors the solid state transformation pathway as discussed above. Thus, goethite remained the only oxidation product for $Q = 0.88$. This finding is consistent with previous work, which correlated the proportions of Fe_3O_4 and FeOOH compounds in the rust layer with the Cr content of low alloy steels[56]. It was demonstrated that for 4–8 wt% Cr, the resistance to atmospheric corrosion was improved because Cr promoted the formation of FeOOH and decreased the proportion of magnetite.

From these results, some conclusions can be drawn about the influence of Cr on marine corrosion of low alloy steel.

In the case of steel permanently immersed in seawater, which is the main topic addressed here, the influence of Cr may be beneficial in the case of a uniform corrosion process, where the Q ratio is expected to be around 1. Cr should favor the formation of non-conductive FeOOH compounds at the detriment of the conductive Fe_3O_4 and thus decrease the risk of formation of corrosion cells, as described in previous work[56]. A higher FeOOH to Fe_3O_4 ratio was also observed for the corrosion product layer formed on 1 wt% Cr + 0.5 wt% Al low alloy steel after permanent immersion in stagnant artificial seawater[6]. In laboratory conditions or in artificial seawater, or during the aerobic phase as defined by the phenomenological model of R. Melchers for natural exposure conditions[1–4], Cr should then improve the resistance to corrosion of low alloy steel.

The main corrosion products of actual seawater corrosion of steel are GR_{SO4}, magnetite, goethite, lepidocrocite, and, in natural environments, FeS that result from SRB metabolic activity[32]. The oxidation of $Fe(OH)_2$ can lead to each of these compounds, except FeS. The present study gives direct information about the role of Cr on the formation of most of the actual corrosion products, but not on the formation of FeS. However, it demonstrates that Cr hinders the formation of GR compounds. This should favor the formation of other Fe(II)-based compounds. In natural exposure conditions, the formation of FeS should then be favored, as indeed observed in previous work[53]. Because FeS is an electronic conductor, the effect of Cr could then be detrimental once the corrosion process is mainly controlled by SRB activity, i.e., at long-term during the anaerobic phase of the process.

In the case of localized corrosion, both anodic and cathodic zones have to be considered separately. It has been demonstrated that for carbon steel permanently immersed in seawater, the localized corrosion processes could persist because the composition of the corrosion product layer differed in anodic and cathodic zones[31,32,57]. In cathodic zones, the corrosion product layer is enriched in magnetite, an electronic conductor, and depleted in GR_{SO4} and FeOOH phases that are insulators. Consequently, dissolved O_2 can be readily reduced at the corrosion product layer/seawater interface, and the underlying metal surface can act as cathode. Conversely, the anodic zones are depleted in Fe_3O_4 and enriched in GR_{SO4} and FeOOH compounds. Moreover, the corrosion being more active in anodic zones, the corrosion product layer is thicker. Consequently, the corrosion product layer acts as a barrier against O_2 diffusion, increasing the anodic character of the underlying metal surface. In this situation, the effect of Cr may depend on the alloy composition.

For low Cr contents, the effects of Cr should be limited to those highlighted by the present study. In the cathodic zones, where Q should be lower than 1, Cr may favor the formation of poorly crystallized FeOOH phases at the detriment of Fe_3O_4, consequently favoring the formation of a corrosion product layer acting as a barrier against O_2 diffusion. In the anodic zones, where Q should be higher than 1, Cr may hinder the formation of GR compounds hence favor the formation of magnetite. Globally, Cr would induce effects that oppose to the persistence of cathodic and anodic zones. The process describes above involves mainly dissolved O_2 and relates to the aerobic phase of the phenomenological model[1–4].

For larger Cr amounts, the enrichment in Cr at the steel seawater interface may induce the well-known effect of Cr, involved in stainless steel resistance to corrosion, that is a trend to passivation. This trend should be favored in the cathodic zones of the steel surface, where the interfacial pH is increased, so that localized corrosion should be favored, as confirmed by big data analysis in the case of atmospheric corrosion[5]. This phenomenon should also be compared to the formation of Cr oxides or Cr-rich Fe-oxides on the surface of low alloy steels reported in various studies dealing whether with marine corrosion[6,8] or corrosion in other saline solutions[7,9,10]. Such oxides were not observed in the present study which shows that their formation does not result from interactions between $Fe(OH)_2$ and Cr(III) species but involves surface reactions that can lead to the formation of an oxide phase

Table 2. Concentrations (mol L^{-1}) of reactants used for the synthesis of Fe(II)/Cr(III) hydroxide(s).

Experiments	Concentrations of reactants				
	[NaOH]	[NaCl]	[$Na_2SO_4 \cdot 10H_2O$]	[$FeCl_2 \cdot 4H_2O$]	[$CrCl_3 \cdot 6H_2O$]
Cr 0%; $Q = 1$	0.24	0.31	0.03	0.12	0
Cr 0%; $Q = 1.136$	0.211	0.31	0.03	0.12	0
Cr 0%; $Q = 0.88$	0.273	0.31	0.03	0.12	0
Cr 2%; $Q = 1$	0.2424	0.3076	0.03	0.1176	0.0024
Cr 8%; $Q = 1$	0.25	0.30	0.03	0.11	0.01
Cr 8%; $Q = 1.136$	0.22	0.30	0.03	0.11	0.01
Cr 8%; $Q = 0.88$	0.284	0.30	0.03	0.11	0.01

They are expressed with respect to the overall volume of solution (200 mL).

directly on the metal surface, e.g., through a process similar to the formation of a passive oxide film. Such a process does not involve the precipitation of solid compounds in the aqueous phase.

In conclusion, our results are consistent with the conclusions drawn by R. Melchers in its thorough study devoted to the role of alloying elements on the corrosion of low alloy steel in natural seawater[1]. For low Cr amounts, typically Cr < 3 wt%, Cr may be beneficial at short-term (aerobic phase), if associated with Mo or Al, and detrimental at long term (anaerobic phase). The remaining question then relates to the seemingly important role of Al and Mo upon the influence of Cr[1].

METHODS

Preparation and oxidation of $Fe(OH)_2$ aqueous suspensions

$Fe(OH)_2$ was obtained by mixing a 100 mL solution of $FeCl_2 \cdot 4H_2O$, NaCl, and $Na_2SO_4 \cdot 10H_2O$ with a 100 mL solution of NaOH. To study the influence of Cr(III) species, part of $FeCl_2 \cdot 4H_2O$ was replaced by $CrCl_3 \cdot 6H_2O$ so that the proportion in Cr was about 8 at.% (exactly 8.33%). Preliminary experiments were performed with 2 at.% Cr but only some results, obtained with an initial ratio of reactants (see below) $Q = 1$, are presented.

The considered concentrations of reactants are listed in Table 2. They are based on those previously used for the study of the influence of Cr(III) and Al(III) on the precipitation and oxidation of GR_{SO4}[28]. The NaCl and $Na_2SO_4 \cdot 10H_2O$ concentrations were chosen so that the overall Cl^- (0.55 mol L^{-1}) and SO_4^{2-} (0.03 mol L^{-1}) concentrations corresponded to those of seawater[58]. The overall Fe(II)+Cr(III) concentration was set constant at 0.12 mol L^{-1} and the NaOH concentration was then varied to modify the ratio between the reactants. The considered ratio, denoted Q, is defined by the following equation:

$$Q = \frac{2[Fe^{2+}] + 3[Cr^{3+}]}{[OH^-]} \quad (3)$$

With this definition, the value $Q = 1$ corresponds to the stoichiometric conditions of the precipitation of $Fe(OH)_2$ and $Cr(OH)_3$ according to the reaction:

$$Fe^{2+} + xCr^{3+} + (2 + 3x)OH^- \rightarrow Fe(OH)_2 + xCr(OH)_3 \quad (4)$$

In this writing, the main considered experimental conditions, i.e., Cr = 0% and Cr = 8%, correspond to $x = 0$ and $x = 0.087$, respectively. If $Q > 1$, then Fe^{2+} and Cr^{3+} cations are in excess with respect to OH^- ions whereas if $Q < 1$, OH^- ions are in excess. The three cases were considered, with Q values of 1, 1.136, and 0.88. Note that the stoichiometric conditions are the same whether Cr(III) precipitates as $Cr(OH)_3$, CrOOH or Cr_2O_3, e.g.,:

$$Fe^{2+} + xCr^{3+} + (2 + 3x)OH^- \rightarrow Fe(OH)_2 + xCrOOH + xH_2O \quad (5)$$

The solutions were not deaerated and were mixed in air, stirred ~30 s without specific precaution, so that a small proportion of Fe(II) may have been oxidized during the precipitation process. However, the amount of dissolved oxygen initially present is negligible with respect to the overall amount of Fe(II), as large concentrations are used (0.11 and 0.12 mol L^{-1}). Then, once the precipitation was achieved:

(1) The obtained aqueous suspension was oxidized completely. In this case, the oxidation of the precipitate was achieved by a magnetic stirring (470 rpm, rod 4-cm long and 6-mm diameter) of the suspension in open air, which ensured a progressive homogeneous process. The 200 mL suspension was aerated at the liquid-air interface in a beaker of 9-cm diameter set in a thermostatic bath at a controlled temperature of 25 ± 0.5 °C. The oxidation reaction was monitored by recording the potential E of a platinum electrode immersed in solution, using an Ag-AgCl-3M electrode as a reference ($E = +0.210$ V vs SHE at 25 °C). The E vs time curves were acquired using a VSP Bio-Logic potentiostat.

(2) The obtained aqueous suspension was poured in a sealed flask, filled to the rim so that no air remains and aged 1 week before FT-IR spectroscopy analysis under N_2 atmosphere. The procedure used to avoid the oxidation of the precipitate was already used previously[45] and is described thereafter.

(3) The obtained suspension was aged 1 week in anoxic conditions as described above, to increase the crystallinity of the precipitated solid phases and allow an in situ XRD monitoring of the oxidation of thin compact layers of $Fe(OH)_2$.

Characterization of the $Fe(OH)_2$ precipitates

The $Fe(OH)_2$ precipitates were characterized by FT-IR spectroscopy using a Thermo-Nicolet iS50 spectrometer equipped with a KBr beamsplitter, a DTGS detector, and an attenuated total reflectance (ATR) iTX accessory with diamond crystal.

A small amount of the aqueous suspension to be studied was rapidly filtered (a few seconds). The obtained slightly wet paste was then rinsed with ethanol, sampled with a spatula and spread on the diamond crystal of the ATR accessory. The sample holder was covered with a hemispheric plastic cell insulating it and allowing a nitrogen flow to pass through. After a complete evaporation of the ethanol and, if possible (see section "Results"), of the water remaining in the sample, which was controlled via the previsualization function of the data collecting and processing

associated software (OMNIC), the acquisition of the spectrum was carried out with 128 scans at a resolution of 8 cm^{-1}. This resolution was sufficient to distinguish all the characteristic vibration bands of $Fe(OH)_2$ and was chosen to minimize the acquisition time.

A background spectrum was acquired each hour and used for all samples studied within this hour. Like those of the samples, the background spectra were acquired under nitrogen flow.

Characterization of the oxidation products of $Fe(OH)_2$ aqueous suspensions

The end products of the oxidation of aqueous suspensions of $Fe(OH)_2$ were filtered, air-dried, and finely crushed in an agate mortar for μRS and XRD analysis. A Horiba High Resolution Raman spectrometer (LabRAM HR) equipped with a microscope (Olympus BX 41) and a Peltier-based cooled charge coupled device (CCD) detector was used for μRS analysis. The zones analyzed through a ×50 objective had a diameter of ~5 μm. Spectra were recorded at room temperature with a resolution of ~0.1 cm^{-1}. Excitation was provided by a green laser diode (533 nm) whose power was reduced to 2.5% of the maximum (~0.5 mW) in order to prevent an excessive heating able to induce the transformation of the analyzed Fe-compound into α-Fe_2O_3 (hematite)[39]. The acquisition time was 1 min in most cases, but was increased up to 2 min when necessary to optimise the signal-to-noise ratio.

The XRD analysis was performed with a Thermo Scientific ARL-INEL EQUINOX 6000 diffractometer using Co-Kα radiation (λ = 0.17903 nm). The system is equipped with a curved detector (CPS-590) designed for the simultaneous detection of the diffracted photons on a 2θ range of 90°. The acquisition of each XRD pattern was made with a constant angle of incidence (7°) during 45 min.

XRD monitoring of the oxidation of thin layers of $Fe(OH)_2$

The XRD monitoring was carried out with the Thermo Scientific ARL-INEL EQUINOX 6000 diffractometer also used for the characterization of the final oxidation products, since it allows to record the XRD pattern obtained on a 90° 2θ-range at any time.

The suspension to be studied was filtered while sheltered from air with a plastic membrane during the process. The obtained wet paste was mixed with a few droplets of glycerol, a procedure initially designed to prevent the oxidation by O_2 of GR compounds[59]. The resulting oily wet paste was then set in the sample holder of the XRD system, thus forming a 280 μm thick compact layer.

The first preliminary tests demonstrated that, depending on the remaining water content of the paste obtained after filtration and the additional amount of glycerol, the oxidation process could be only slowed down and not totally hindered. Consequently, this process could be monitored in situ using XRD. For that purpose, an XRD pattern was recorded after different increasing acquisition times, namely 30 s, 3, 13, and 30 min.

The various phases were identified via the ICDD (International Center for Diffraction Data) PDF-4 database. The files used for the various compounds were 01-073-6991 and 00-013-0089 for Fe(II)-hydroxide, 00-029-0713 (goethite), 01-044-1415 (lepidocrocite), 01-082-1533 (magnetite), 01-077-0247 (feroxyhyte), 00-040-0127 (chloride green rust), 01-074-3400 (sulfate green rust), 00-005-0628 (halite, i.e., NaCl) and 00-016-0817 ($Cr(OH)_3 \cdot 6H_2O$). The diffraction lines of sulfate green rust, chloride green rust, and feroxyhyte were, however, indexed according to the reported studies of their crystal structures[34,38,46,48,50].

DATA AVAILABILITY

The data that support the findings of this study are available in "figshare" with the identifier https://doi.org/10.6084/m9.figshare.24847767.

Received: 19 October 2023; Accepted: 26 December 2023;
Published online: 06 January 2024

REFERENCES

1. Melchers, R. E. Effect of small compositional changes on marine immersion corrosion of low alloy steels. *Corros. Sci.* **46**, 1669–1694 (2004).
2. Melchers, R. E. Mathematical modelling of the diffusion-controlled phase in marine immersion corrosion of mild steel. *Corros. Sci.* **45**, 923–940 (2003).
3. Melchers, R. E. & Jeffrey, R. Early corrosion of mild steel in seawater. *Corros. Sci.* **47**, 1678–1693 (2005).
4. Melchers, R. E. & Wells, T. Models for the anaerobic phases of marine immersion corrosion. *Corros. Sci.* **48**, 1791–1811 (2006).
5. Yang, X. et al. A new understanding of the effect of Cr on the corrosion resistance evolution of weathering steel based on big data technology. *J. Mater Sci. Technol.* **104**, 67–80 (2022).
6. Refait, Ph., Jeannin, M., Urios, T., Fagot, A. & Sabot, R. Corrosion of low alloy steel in stagnant artificial or stirred natural seawater: role of Al and Cr. *Mater. Corros.* **70**, 985–995 (2019).
7. Li, J. et al. Corrosion behavior of low-carbon Cr micro-alloyed steel for grounding grids in simulated acidic soil. *J. Iron Steel Res. Int.* **25**, 755–766 (2018).
8. Yang, J., Jiang, S. & Xu, F. Effect of Cr on the characteristic of rust layer formed on low alloy steels immersed in flowing 3.5%NaCl solution. *J. Phys.: Conf. Ser.* **1626**, 012175 (2020).
9. Hao, X. et al. The microstructure and corrosion behavior of Cr-containing ferrite-pearlite steels in acidic environment. *Anti-Corros. Methods Mater.* **70**, 218–226 (2023).
10. Park, J. S., Lee, S. C., Choi, J. K. & Kim, S. J. Advanced Hadfield steel with Cr-optimization resists against corrosion and erosion-corrosion. *Appl. Surf. Sci.* **637**, 157875 (2023).
11. Yamashita, M., Miyuki, H., Matsuda, Y., Nagano, H. & Misawa, T. The long term growth of the protective rust layer formed on weathering steel by atmospheric corrosion during a quarter of a century. *Corros. Sci.* **36**, 283–299 (1994).
12. Nishimura, T. Rust formation mechanism on low alloy steels after exposure test in high Cl^- and high SO_x environment. *Materials* **10**, 199 (2017).
13. Jiang, S., Chai & Yang, C. F. Influence of Cr on reduction behavior of rust formed on low alloy steels in flowing 3.5% NaCl solution. *J. Iron Steel Res.* **30**, 251–258 (2018).
14. Wu, X.-J. et al. Initial corrosion behavior and electrochemical property evolution of 40CrNiMo steel in salt spray environment. *Surf. Technol.* **51**, 234–244 (2022).
15. Ming, J., Zhou, X., Jiang, L. & Shi, J. Corrosion resistance of low-alloy steel in concrete subjected to long-term chloride attack: Characterization of surface conditions and rust layers. *Corros. Sci.* **203**, 110370 (2022).
16. Qi, X. et al. Corrosion resistance and mechanism of X100 pipeline steel laser-metal active gas hybrid welds with Cr containing welding wire in NS_4 solution. *Corros. Sci.* **221**, 111329 (2023).
17. Cho, S.-W. et al. Effect of Cr on aqueous and atmospheric corrosion of automotive carbon steel. *Materials* **14**, 2444 (2021).
18. Yuan, R., Wu, H. & Gu, Y. Effect of alloyed Cr on corrosion behavior of low-alloy steel in wet atmosphere. *Mater. Corros.* **73**, 918–931 (2022).
19. Liu, W. et al. Role of Cr in the anticorrosion ability of weathering steel based on the microcharacteristics of synthetic α-FeOOH in the presence of Cr(III). *JOM* **75**, 3170–3182 (2023).
20. Dong, B. et al. Corrosion failure analysis of low alloy steel and carbon steel rebar in tropical marine atmospheric environment: Outdoor exposure and indoor test. *Eng. Fail. Analy.* **19**, 105720 (2021).
21. Dong, B. et al. Optimize Ni, Cu, Mo element of low Cr-steel rebars in tropical marine atmosphere environment through two years of corrosion monitoring. *Cem. Concrete Comp.* **125**, 104317 (2022).
22. Cook, D. C. Spectroscopic identification of protective and non-protective coatings on steel structures in marine environments. *Corros. Sci.* **47**, 2250–2570 (2005).
23. Suzuki, S. et al. Influence of chromium on the local structure and morphology of ferric oxyhydroxides. *Corros. Sci.* **46**, 1751–1763 (2004).
24. Asamai, K. & Kikuchi, M. In-depth distribution of rusts on a plain carbon steel and weathering steels, exposed to coastal-industrial atmosphere for 17 years. *Corros. Sci.* **45**, 2671–2688 (2003).
25. Stratmann, M. & Hoffmann, K. In situ Mössbauer spectroscopic study of reactions within rust layers. *Corros. Sci.* **29**, 1329–1352 (1989).
26. Kamimura, T., Hara, S., Miyuki, H., Yamashita, M. & Uchida, H. Composition and protective ability of rust layer formed on weathering steel exposed to various environments. *Corros. Sci.* **48**, 2799–2812 (2006).
27. Inoue, K., Shinoda, K., Susuki, S. & Waseda, Y. Oxidation of green rust suspensions containing different chromium ion species. *Corros. Sci.* **52**, 1421–1427 (2010).

28. Refait, Ph., Sabot, R. & Jeannin, M. Role of Al(III) and Cr(III) on the formation and oxidation of the Fe(II-III) hydroxysulfate Green Rust. *Coll. Surf. A* **531**, 203–212 (2017).
29. Pineau, S. et al. Formation of the Fe(II-III) hydroxysulphate green rust during marine corrosion of steel associated to molecular detection of dissimilatory sulphite-reductase. *Corros. Sci.* **50**, 1099–1111 (2008).
30. Refait, Ph. et al. Electrochemical formation of green rusts in deaerated seawater-like solutions. *Electrochim. Acta* **56**, 6481–6488 (2011).
31. Refait, Ph., Grolleau, A.-M., Jeannin, M., François, E. & Sabot, R. Localized corrosion of carbon steel in marine media: galvanic coupling and heterogeneity of the corrosion product layer. *Corros. Sci.* **111**, 583–595 (2016).
32. Refait, Ph., Grolleau, A.-M., Jeannin, M., Rémazeilles, C. & Sabot, R. Corrosion of carbon steel in marine environments: role of the corrosion product layer. *Corros. Mater. Degrad.* **1**, 198–218 (2020).
33. Refait, Ph. & Génin, J.-M. R. The oxidation of ferrous hydroxide in chloride-containing aqueous media and Pourbaix diagrams of Green Rust One. *Corros. Sci.* **34**, 797–819 (1993).
34. Refait, Ph., Abdelmoula, M. & Génin, J.-M. R. Mechanisms of formation and structure of green rust one in aqueous corrosion of iron in the presence of chloride ions. *Corros. Sci.* **40**, 1547–1560 (1998).
35. Olowe, A. A. & Génin, J.-M. R. The mechanism of oxidation of Fe(II) hydroxide in sulfated aqueous media: importance of the initial ratio of the reactants. *Corros. Sci.* **32**, 965–984 (1991).
36. Génin, J.-M. R., Olowe, A. A., Refait, Ph. & Simon, L. On the stoichiometry and Pourbaix diagram of Fe(II)-Fe(III) hydroxy-sulphate or sulphate-containing green rust 2; an electrochemical and Mössbauer spectroscopy study. *Corros. Sci.* **38**, 1751–1762 (1996).
37. Refait, Ph. & Génin, J.-M. R. The transformation of chloride-containing green rust 1 into sulphated green rust 2 by oxidation in mixed Cl^-/SO_4^{2-} aqueous media. *Corros. Sci.* **36**, 55–65 (1994).
38. Simon, L. et al. Structure of the Fe(II-III) layered double hydroxysulphate green rust two from Rietveld analysis. *Sol. State Sci.* **5**, 327–334 (2003).
39. De Faria, D. L. A., Silva, S. V. & Oliveira, M. T. D. Raman micro spectroscopy study of some iron oxides and oxyhydroxides. *J. Raman Spectrosc.* **28**, 873–878 (1997).
40. Neff, D., Dillmann, P., Bellot-Gurlet, L. & Béranger, G. Corrosion of iron archaeological artefacts in soil: characterisation of the corrosion system. *Corros. Sci.* **47**, 515–535 (2005).
41. Monnier, J. et al. A corrosion study of the ferrous medieval reinforcement of the Amiens cathedral. Phase characterisation and localisation by various microprobes techniques. *Corros. Sci.* **52**, 695–710 (2010).
42. Libnau, F. O., Kvalheim, O. M., Christy, A. A. & Toft, J. Spectra of water in the near- and mid-infrared region. *Vibr. Spectrosc.* **7**, 243–254 (1994).
43. Lane, M. D. Mid-infrared emission spectroscopy of sulfate and sulfate-bearing minerals. *Amer. Miner.* **92**, 1–18 (2007).
44. Lutz, H. D., Möller, H. & Schmidt, M. Lattice vibration spectra. Part LXXXII. Brucite-type hydroxides $M(OH)_2$ (M = Ca, Mn, Co, Fe, Cd) – IR and Raman spectra, neutron diffraction of $Fe(OH)_2$. *J. Mol. Struct.* **328**, 121–132 (1994).
45. Duboscq, J., Abdelmoula, M., Jeannin, M., Sabot, R. & Refait, Ph. On the formation and transformation of Fe(III)-containing chukanovite, $Fe^{II}_{2-x}Fe^{III}_x(OH)_{2-x}O_xCO_3$. *J. Phys. Chem. Solids* **138**, 109310 (2020).
46. Francombe, M. H. & Rooksby, H. P. Structure transformations effected by the dehydration of diaspore, goethite and delta ferric oxide. *Clay Min. Bull.* **4**, 1–14 (1959).
47. Muller, O., Wilson, R. & Krakow, W. δ-FeO(OH) and its solid solutions—Part 1: Preparation and crystal chemistry. *J. Mater. Sci.* **14**, 2929–2936 (1979).
48. Drits, V. A., Sakharov, B. A. & Manceau, A. Structure of feroxyhite as determined by simulation of X-ray diffraction curves. *Clay Miner.* **28**, 209–222 (1993).
49. Olowe, A. A., Refait, Ph. & Génin, J.-M. R. Influence of concentration on the oxidation of ferrous hydroxide in basic sulphated aqueous medium: particle size analysis of goethite and delta FeOOH. *Corros. Sci.* **32**, 1003–1020 (1991).
50. Sestu, M., Carta, D., Casula, M. F., Corrias, A. & Navarra, G. Novel interpretation of the mean structure of feroxyhyte. *J. Sol. State Chem.* **225**, 256–260 (2015).
51. Drits, V. A., Sakharov, B. A., Salyn, A. L. & Manceau, A. Structural model for ferrihydrite. *Clay Miner.* **28**, 185–207 (1993).
52. Shannon, R. D. Revised effective ionic radii and systematic studies of interatomic distances in halides and chalcogenides. *Acta cryst.* **A32**, 751–767 (1976).
53. Malard, E., Kervadec, D., Gil, O., Lefevre, Y. & Malard, S. Interactions between steels and sulphide-producing bacteria-Corrosion of carbon steels and low-alloy steels in natural seawater. *Electrochim. Acta* **54**, 8–13 (2008).
54. Leidheiser, H. & Czako-Nagy, I. A Mössbauer spectroscopic study of rust formed during simulated atmospheric corrosion. *Corros. Sci.* **24**, 569–577 (1984).
55. Kelsall, G. H. & Williams, R. A. Electrochemical behavior of ferrosilicides (FexSi) in neutral and alkaline aqueous electrolytes. I. Thermodynamics of Fe-Si-H_2O systems at 298 K. *J. Electrochem. Soc.* **138**, 931–940 (1991).
56. Sun, B., Zuo, X. & Li, X. The role of chromium content in the long-term atmospheric corrosion process. *npj Mater. Degrad.* **4**, 37 (2020).
57. Refait, Ph., Jeannin, M., François, E., Sabot, R. & Grolleau, A.-M. Galvanic corrosion in marine environments: effects associated with the inversion of polarity of Zn/carbon steel couples. *Mater. Corros.* **70**, 950–961 (2019).
58. Riley, J. P. & Chester, R. *Introduction to Marine Chemistry*. (Academic Press, 1971).
59. Hansen, H. C. B. Composition, stabilisation, and light absorption of Fe(II)-Fe(III) hydroxycarbonate (green rust). *Clay Miner.* **24**, 663–669 (1989).

ACKNOWLEDGEMENTS

The authors thank Ms Khadidiatou Diallo, Master degree student, for her help during part of the experimental work.

AUTHOR CONTRIBUTIONS

M.S.: Measurements, data analysis, methodology, visualization; C.R.: Measurements, conceptualization, data analysis, methodology, funding acquisition; P.R.: Measurements, conceptualization, data analysis, visualization, methodology, writing, funding acquisition.

COMPETING INTERESTS

The authors declare no competing interests.

ADDITIONAL INFORMATION

Supplementary information The online version contains supplementary material available at https://doi.org/10.1038/s41529-023-00424-8.

Correspondence and requests for materials should be addressed to Ph Refait.

Reprints and permission information is available at http://www.nature.com/reprints

Publisher's note Springer Nature remains neutral with regard to jurisdictional claims in published maps and institutional affiliations.